Tracer transport: A new multi-tracer scheme, a new idealized test case suite, and a new methodology for quantifying numerical mixing

Peter Hjort Lauritzen

Atmospheric Modeling & Predictability Section
Climate & Global Dynamics Division
National Center for Atmospheric Research, Boulder, Colorado

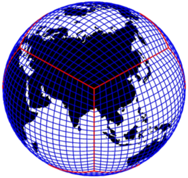

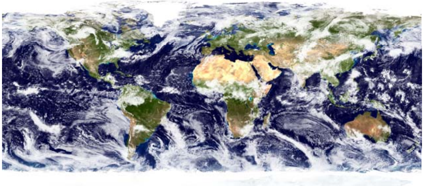

Collaborators: R.Nair (IMAGe), J.Thuburn (U.Exeter), L.Harris† (GFDL),P.Ullrich† (UMICH), M. Taylor (Sandia), C.Jablonowski (UMICH), R.Mittal (MMM), C. Erath (CU/NCAR)

† former SIParCS student (SIParCS = R. Loft's Summer Internships in Parallel Computational Science program)

1. Motivation: Why focus on tracer transport? (context: global climate models)
2. Conservative Semi-LAgrangian Multi-tracer (CSLAM) scheme
   - scheme basics ('Lagrangian' version)
   - flux-form version of CSLAM (FF-CSLAM)
   - experimentation with limiters/filters
   - simplified FF-CSLAM
3. Commercial break
4. New challenging test cases for transport schemes on the sphere
   - analytic winds and initial conditions (analytical solution)
5. Preserving pre-existing functional relations between tracers
   - mixing diagnostics
   - example application: new test case with interrelated tracers
6. Commercial break
7. Future directions

Why focus on transport schemes? Multi-tracer efficiency

Continuity equations in NCAR's Community Atmosphere Model (CAM) version 5

- Air density
- Water species: Water vapor, cloud liquid water and ice
- Microphysics & Aerosols: number concentrations (cloud water variables, aerosols), particulate organic matter, dust, sea salt, secondary organic aerosols, ... (**total of 22**)

Continuity equations in Chemistry version of CAM

Prognoses 126+ chemical species (Lamarque et al., 2008)

$\hookrightarrow$ *In many atmospheric modeling applications the computational cost of resolved dynamics is (or is expected to be) dominated by the cost of tracer transport*

$\hookrightarrow$ *Multi-tracer efficiency is becoming increasingly important*

Why focus on transport schemes? Accuracy on 'fancy grids'

regular latitude-longitude

cubed-sphere

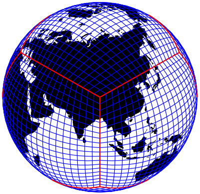

Voronoi

Yin-Yang

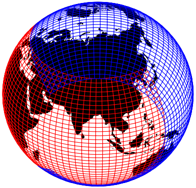

Primarily for scalability many groups are considering more isotropic spherical grids $\rightarrow$ challenges schemes in new ways:

- Grids are not orthogonal (at least not globally):
- $\Rightarrow$ potential loss of accuracy with dimensionally split schemes
- Balanced flows are newer always aligned with grid lines; has consequences for maintaining large scale balances in the flow at low resolution;

  Lauritzen, Jablonowski, Taylor, Nair (2010a, Journal of Advances in Modeling Earth Systems)
- 'Geometrically flexible' schemes desirable for 'fancy grids', mesh-refinement, etc.

Example from CAM5 at $1.9^\circ \times 2.5^\circ$ resolution

Water variables

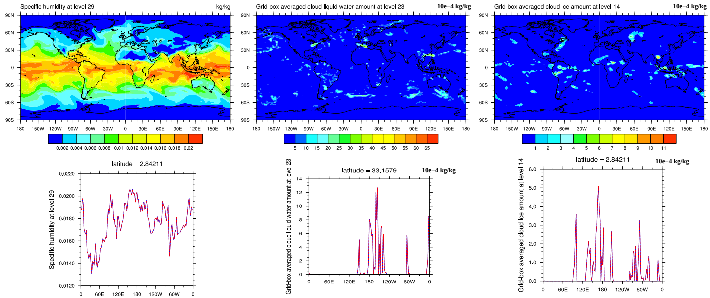

- many fields (water variables, aerosols, chemical species, ...) contain near grid-scale features
- production/loss terms are large, however, locally the advective tendency can be large (e.g., cloud ice mixing ratio for Cirrus, aerosols, ...)

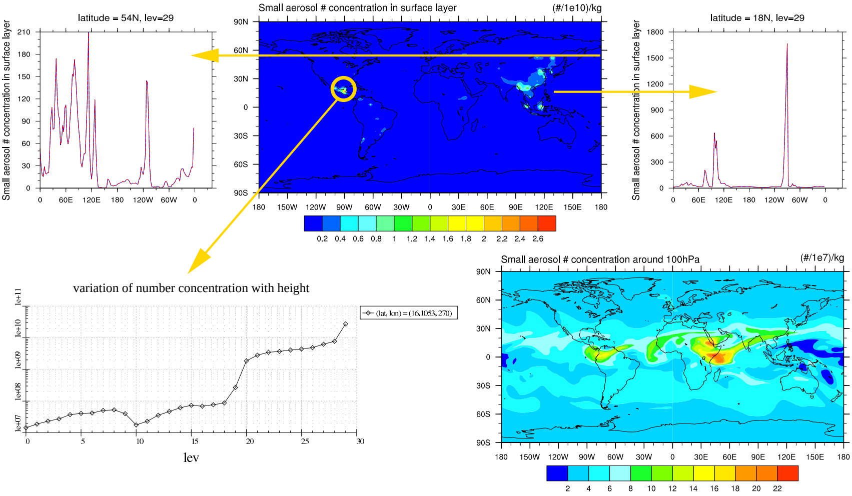

Data for these Figures provided by J.F. Lamarque

Part I

New geometrically flexible multi-tracer scheme

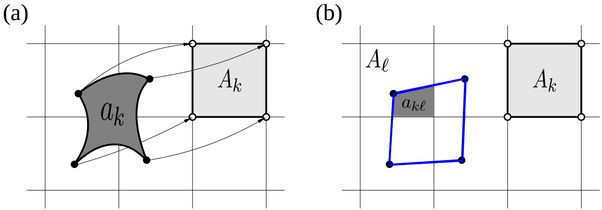

Finite-volume Lagrangian form of continuity equation for $\psi = \rho, \rho\,\phi$:

$$\int_{A_k} \psi_k^{n+1}\, dx\, dy = \int_{a_k} \psi_k^{n}\, dx\, dy \quad = \quad \sum_{\ell=1}^{L_k} \iint_{a_{k\ell}} f_\ell(x,y)\, dx\, dy,$$

where the $a_{k\ell}$'s are non-empty overlap regions:

$$a_{k\ell} = a_k \cap A_\ell, \quad a_{k\ell} \neq \emptyset; \quad \ell = 1, \ldots, L_k. \tag{1}$$

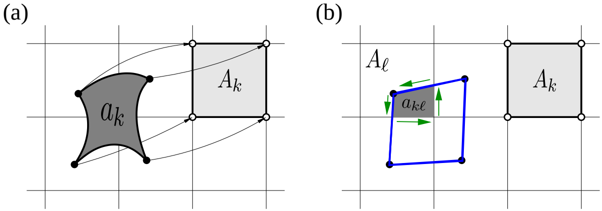

Finite-volume Lagrangian form of continuity equation for $\psi = \rho, \rho\,\phi$:

$$\int_{A_k} \psi_k^{n+1}\, dx\, dy = \int_{a_k} \psi_k^n \, dx\, dy \quad = \quad \sum_{\ell=1}^{L_k} \oint_{\partial a_{k\ell}} \left[P\, dx + Q\, dy \right],$$

where $\partial a_{k\ell}$ is the boundary of $a_{k\ell}$ and

$$-\frac{\partial P}{\partial y} + \frac{\partial Q}{\partial x} = f_\ell(x,y) = \sum_{i+j\leqslant 2} c_\ell^{(i,j)} x^i y^j .$$

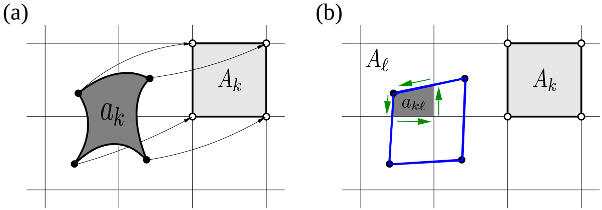

Finite-volume Lagrangian form of continuity equation for $\psi = \rho, \rho\,\phi$:

$$\int_{A_k} \psi_k^{n+1}\, dx\, dy = \int_{a_k} \psi_k^n\, dx\, dy \quad = \quad \sum_{\ell=1}^{L_k} \left[\sum_{i+j\leqslant 2} c_\ell^{(i,j)} w_{k\ell}^{(i,j)} \right],$$

where weights $w_{k\ell}^{(i,j)}$ are functions of the coordinates of the vertices of $a_{k\ell}$.

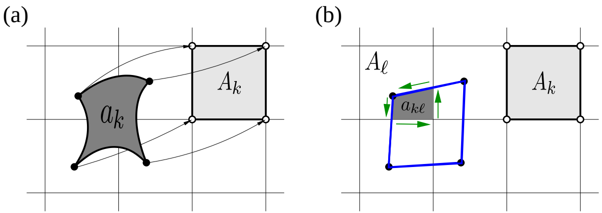

Finite-volume Lagrangian form of continuity equation for $\psi = \rho, \rho\,\phi$:

$$\int_{A_k} \psi_k^{n+1}\,dx\,dy = \int_{a_k} \psi_k^{n}\,dx\,dy \quad = \quad \sum_{\ell=1}^{L_k} \left[\sum_{i+j\leqslant 2} c_\ell^{(i,j)} w_{k\ell}^{(i,j)} \right],$$

- $w_{k\ell}^{(i,j)}$ can be re-used for each additional tracer (Dukowicz and Baumgardner, 2000)
- computational cost for each additional tracer is the reconstruction and limiting/filtering.
- CSLAM is stable for long time-steps (CFL$>$1)

- CSLAM is fully two-dimensional and can be extended to any spherical grid constructed from great-circle arcs.
- Cubed-sphere extension of CSLAM is discussed in detail in Lauritzen, Nair, Ullrich (2010,JCP)
- Extension of CSLAM to icosahedral grids discussed in Mittal and Lauritzen (2010, in prep)

Flux-form CSLAM (FF-CSLAM); Harris,Lauritzen,Mittal (2010,JCP)

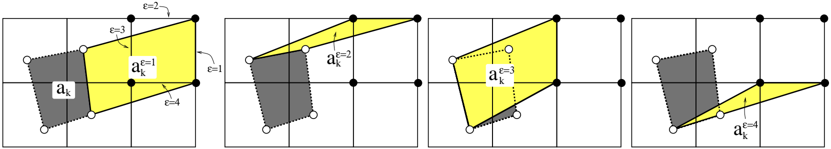

Finite-volume flux-form of continuity equation for $\psi = \rho, \rho\,\phi$:

$$\int_{A_k} \psi_k^{n+1}\, dx\, dy = \int_{A_k} \psi_k^{n}\, dx\, dy - \sum_{\epsilon=1}^{4} \left[\sum_{\ell=1}^{L_k^\epsilon} s_{k\ell}^{\epsilon} \iint_{a_{k\ell}^{\epsilon}} f_\ell(x,y)\, dx\, dy \right], \tag{1}$$

where

- a_k^ϵ = 'flux-area' (yellow area) = area swept through face ϵ
- L_k^ϵ = number of overlap areas for a_k^ϵ; $a_{k\ell}^\epsilon = a_k^\epsilon \cap A_k$
- $s_{k\ell}^\epsilon$ = 1 for outflow and -1 for inflow.
- **All technology developed for CSLAM can be re-used**

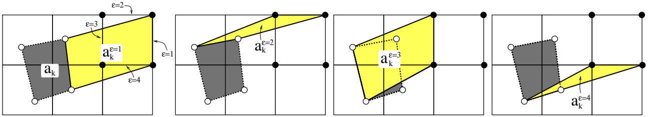

Finite-volume flux-form of continuity equation for $\psi = \rho, \rho\,\phi$:

$$\int_{A_k} \psi_k^{n+1}\,dx\,dy \quad = \quad \int_{A_k} \psi_k^n\,dx\,dy - \sum_{\epsilon=1}^{4}\left[\sum_{\ell=1}^{L_k^\epsilon} s_{k\ell}^\epsilon \iint_{a_{k\ell}^\epsilon} f_\ell(x,y)\,dx\,dy\right], \tag{1}$$

Note: all the areas involved in forecast (1) 'sum-up to' upstream Lagrangian area δa_k:

$$\Delta A_k - \sum_{\epsilon=1}^{4}\left[\sum_{\ell=1}^{L_k^\epsilon} s_{k\ell}^\epsilon \delta a_k^\epsilon\right] = \delta a_k. \tag{2}$$

Aside: in flux-form you'll conserve mass even when you are 'sloppy' about approximating a_k^ϵ, that is, effective upstream areas δa_k do not need to span the domain without overlaps/gaps as for the Lagrangian scheme! (**However, for consistency and maybe accuracy it should be the case**)

$\Rightarrow$ unlimited FF-CSLAM = unlimited CSLAM

$\rightarrow$ **Why FF-CSLAM?**

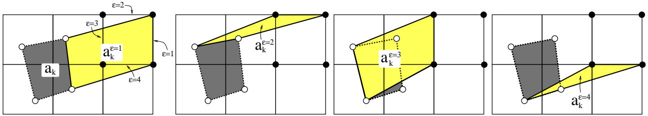

Finite-volume flux-form of continuity equation for $\psi = \rho, \rho\,\phi$:

$$\int_{A_k} \psi_k^{n+1}\, dx\, dy \quad = \quad \int_{A_k} \psi_k^{n}\, dx\, dy - \sum_{\epsilon=1}^{4} \left[\sum_{\ell=1}^{L_k^\epsilon} s_{k\ell}^{\epsilon} \iint_{a_{k\ell}^{\epsilon}} f_\ell(x,y)\, dx\, dy \right], \tag{1}$$

- You get mass-conservation no matter how you approximate fluxes!
- In CSLAM **shape-preservation** is enforced by filtering the sub-grid-cell reconstructions (also applicable for FF-CSLAM)
- Casting in flux-form one may also apply **flux-limiters** such as FCT (Flux-Correct-Transport, Zalesak 1979).
- Flux-form allows for **super-cycling (also referred to as sub-cycling)**, that is, transport tracers with longer time-steps than what is used for the dynamics.
- Drawback: For CFL>1 FF-CSLAM is significantly more expensive than CSLAM

Limiters and filters

- **In the literature: Many 1D limiters but few fully 2D limiters!**
- A priori ('**Monotone filtering**'): Filter the reconstruction $f_\ell(x, y)$ so that extreme values lie within the adjacent cell-average values (Barth and Jespersen, 1989).

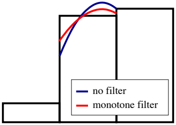

- A posteriori ('**Monotone limiting**'): Limit the fluxes to prevent new extrema in $\overline{\psi}^{n+1}$ using flux-corrected transport (Zalesak, 1979).
- Monotone filters/limiters tend to 'clip' physical extrema

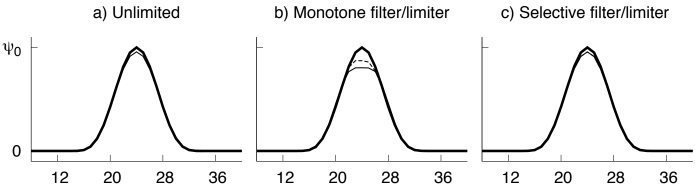

- **In the literature: Many 1D limiters but few fully 2D limiters!**
- A priori ('**Monotone filtering**'): Filter the reconstruction $f_\ell(x,y)$ so that extreme values lie within the adjacent cell-average values (Barth and Jespersen, 1989).

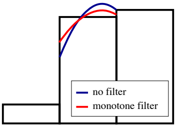

- A posteriori ('**Monotone limiting**'): Limit the fluxes to prevent new extrema in $\overline{\psi}^{n+1}$ using flux-corrected transport (Zalesak, 1979).
- **Selective filtering/selective limiting** (Blossey and Durran, 2008): apply filtering or limiting only where a WENO-based smoothness metric exceeds a certain threshold:

$$\gamma = \frac{1}{2}\left[\left(2\Delta x\frac{\partial f}{\partial x}\right)^2 + \left(\Delta x^2\frac{\partial^2 f}{\partial x^2}\right)^2 + \left(2\Delta y\frac{\partial f}{\partial y}\right)^2 + \left(\Delta y^2\frac{\partial^2 f}{\partial y^2}\right)^2 + \left(\Delta x\Delta y\frac{\partial^2 f}{\partial x\partial y}\right)^2\right] \quad (2)$$

Will render solution non-oscillatory but not strictly monotone ('miniscule' under- and over-shoots)

- **In the literature: Many 1D limiters but few fully 2D limiters!**
- A priori ('**Monotone filtering**'): Filter the reconstruction $f_\ell(x, y)$ so that extreme values lie within the adjacent cell-average values (Barth and Jespersen, 1989).

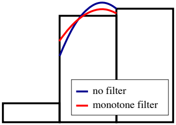

- A posteriori ('**Monotone limiting**'): Limit the fluxes to prevent new extrema in $\overline{\psi}^{n+1}$ using flux-corrected transport (Zalesak, 1979).
- Monotone filters/limiters tend to 'clip' physical extrema

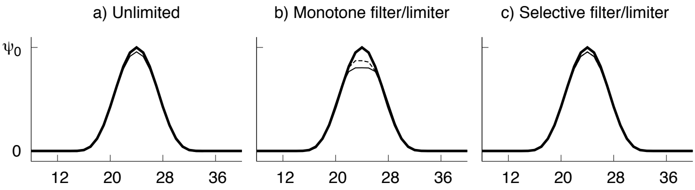

Flux-form CSLAM (FF-CSLAM): Results

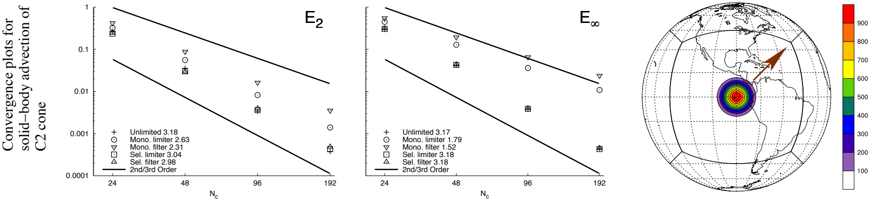

- third-order convergence in E_2 and E_∞ for unlimited scheme and when using selective limiter/filter (for cubed-sphere version of CSLAM)
- for icosahedral grid implementation the convergence rates are closer to second than third-order (least squares reconstruction)!

- a robust search algorithm for overlap areas can be cumbersome to code (although by no means impossible; and the cost of the search will become marginal for a large number of transported tracers)
- what if we get rid of the search for overlap areas?

Simplified FF-CSLAM (Lauritzen,Erath,Mittal,in prep.)

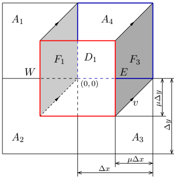

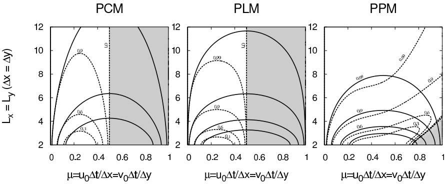

- For the flux-integral for a particular face only the reconstruction in the cell upstream is used (no search needed)

$$e_{sta} = i\,h^3\mu(1-\mu)(k+l) + \mathcal{O}(h^4) \quad and \quad e_{sim} = i\,h^3\mu(1-2\mu)(k+l) + \mathcal{O}(h^4).$$

Simplified FF-CSLAM (Lauritzen,Erath,Mittal,in prep.)

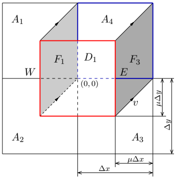

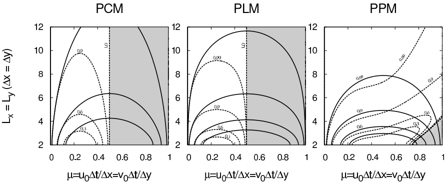

- For the flux-integral for a particular face only the reconstruction in the cell upstream is used (no search needed)
- For CFL$\leqslant$0.5 the results in idealized test cases for cubed-sphere FF-CSLAM improved slightly in terms of standard error norms.
  Very counterintuitive (less rigorous and cheaper scheme is better?)!

$$e_{sta} = i\,h^3\mu(1-\mu)(k+l) + \mathcal{O}(h^4) \quad and \quad e_{sim} = i\,h^3\mu(1-2\mu)(k+l) + \mathcal{O}(h^4).$$

Simplified FF-CSLAM (Lauritzen,Erath,Mittal,in prep.)

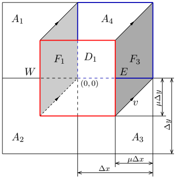

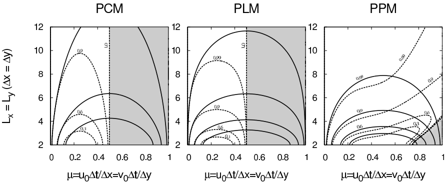

- For the flux-integral for a particular face only the reconstruction in the cell upstream is used (no search needed)
- For CFL$\leqslant$0.5 the results in idealized test cases for cubed-sphere FF-CSLAM improved slightly in terms of standard error norms.
  Very counterintuitive (less rigorous and cheaper scheme is better?)!
- Von Neumann stability analysis for 1^{st},2^{nd}, and 3^{rd} reconstruction functions confirms this!

$$e_{sta} = i\,h^3\mu(1-\mu)(k+l) + \mathcal{O}(h^4) \quad and \quad e_{sim} = i\,h^3\mu(1-2\mu)(k+l) + \mathcal{O}(h^4).$$

Simplified FF-CSLAM (Lauritzen,Erath,Mittal,in prep.)

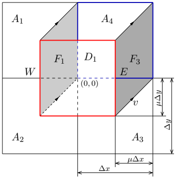

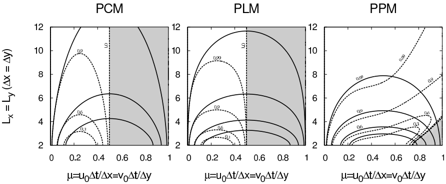

- For the flux-integral for a particular face only the reconstruction in the cell upstream is used (no search needed)
- For CFL$\leqslant$0.5 the results in idealized test cases for cubed-sphere FF-CSLAM improved slightly in terms of standard error norms.
  Very counterintuitive (less rigorous and cheaper scheme is better?)!
- Von Neumann stability analysis for 1^{st},2^{nd}, and 3^{rd} reconstruction functions confirms this!
  - using 1^{st}- and 2^{nd}-order reconstructions the scheme is only stable for CFL$\leqslant$0.5

$$e_{sta} = i\,h^3\mu(1-\mu)(k+l) + \mathcal{O}(h^4) \quad and \quad e_{sim} = i\,h^3\mu(1-2\mu)(k+l) + \mathcal{O}(h^4).$$

Simplified FF-CSLAM (Lauritzen,Erath,Mittal,in prep.)

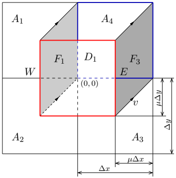

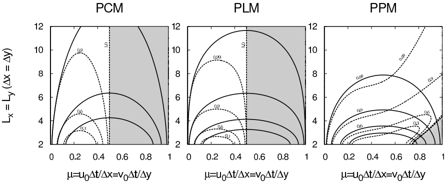

- For the flux-integral for a particular face only the reconstruction in the cell upstream is used (no search needed)
- For CFL$\leqslant$0.5 the results in idealized test cases for cubed-sphere FF-CSLAM improved slightly in terms of standard error norms.
  Very counterintuitive (less rigorous and cheaper scheme is better?)!
- Von Neumann stability analysis for 1^{st},2^{nd}, and 3^{rd} reconstruction functions confirms this!
  - using 1^{st}- and 2^{nd}-order reconstructions the scheme is only stable for CFL$\leqslant$0.5
  - for 3^{rd}-oder reconstruction functions the stability region expands!

$$e_{sta} = i\, h^3 \mu(1-\mu)(k+l) + \mathcal{O}(h^4) \quad and \quad e_{sim} = i\, h^3 \mu(1-2\mu)(k+l) + \mathcal{O}(h^4).$$

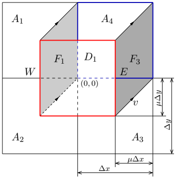

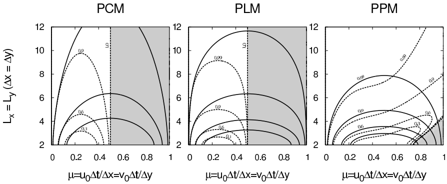

- For the flux-integral for a particular face only the reconstruction in the cell upstream is used (no search needed)
- For CFL⩽0.5 the results in idealized test cases for cubed-sphere FF-CSLAM improved slightly in terms of standard error norms.
  Very counterintuitive (less rigorous and cheaper scheme is better?)!
- Von Neumann stability analysis for 1^{st},2^{nd}, and 3^{rd} reconstruction functions confirms this!
  - using 1^{st}- and 2^{nd}-order reconstructions the scheme is only stable for CFL⩽0.5
  - for 3^{rd}-oder reconstruction functions the stability region expands!
- Error analysis in terms of Taylor series confirms this as well

$$e_{sta} = i\,h^3\mu(1-\mu)(k+l) + \mathcal{O}(h^4) \quad and \quad e_{sim} = i\,h^3\mu(1-2\mu)(k+l) + \mathcal{O}(h^4).$$

CSLAM in CAM-HOMME (High-Order Methods Modeling Environment)

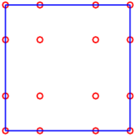

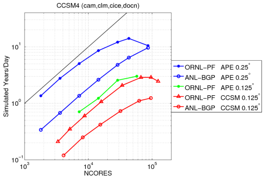

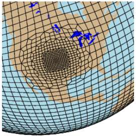

- Scalable spectral element dycore in CAM

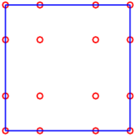

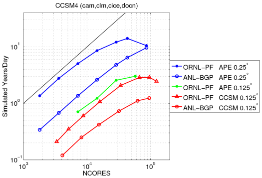

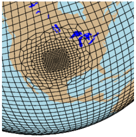

- Scalable spectral element dycore in CAM
  - fully functional with CAM4 physics; soon with mesh-refinement and CAM5 physics

CSLAM in CAM-HOMME (High-Order Methods Modeling Environment)

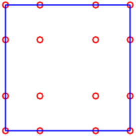

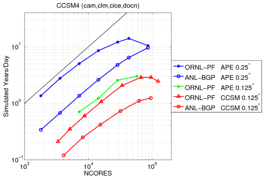

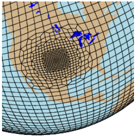

- Scalable spectral element dycore in CAM
  - fully functional with CAM4 physics; soon with mesh-refinement and CAM5 physics
- Conserves total energy to time truncation errors ($\approx 0.014\ W/\mathrm{m}^2$ in $\frac{1}{2}^\circ$ aqua-planet)

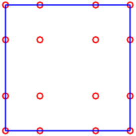

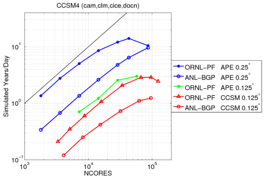

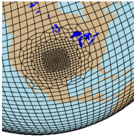

- Scalable spectral element dycore in CAM
  - fully functional with CAM4 physics; soon with mesh-refinement and CAM5 physics
- Conserves total energy to time truncation errors ($\approx$0.014 W/m^2 in $\frac{1}{2}^\circ$ aqua-planet)
- Conserves mass at the element level ('quasi-local')

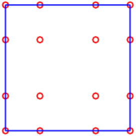

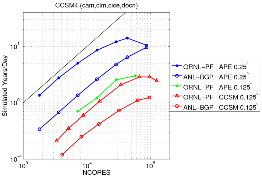

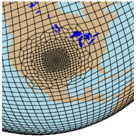

- Scalable spectral element dycore in CAM
  - fully functional with CAM4 physics; soon with mesh-refinement and CAM5 physics
- Conserves total energy to time truncation errors ($\approx$0.014 W/m^2 in $\frac{1}{2}^\circ$ aqua-planet)
- Conserves mass at the element level ('quasi-local')
- Recently filters/limiters have been introduced for shape-preserving tracer transport, however, reduces the transport operator from formally third-order to second-order.

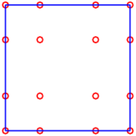

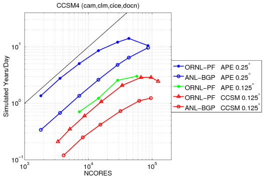

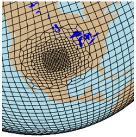

- Scalable spectral element dycore in CAM
  - fully functional with CAM4 physics; soon with mesh-refinement and CAM5 physics
- Conserves total energy to time truncation errors ($\approx$0.014 W/m^2 in $\frac{1}{2}^{\circ}$ aqua-planet)
- Conserves mass at the element level ('quasi-local')
- Recently filters/limiters have been introduced for shape-preserving tracer transport, however, reduces the transport operator from formally third-order to second-order.
- Under DOE grant we are integrating CSLAM into HOMME for tracer transport:

CSLAM in CAM-HOMME (High-Order Methods Modeling Environment)

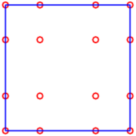

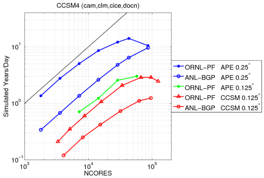

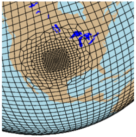

- Scalable spectral element dycore in CAM
  - fully functional with CAM4 physics; soon with mesh-refinement and CAM5 physics
- Conserves total energy to time truncation errors ($\approx$0.014 W/m^2 in $\frac{1}{2}^\circ$ aqua-planet)
- Conserves mass at the element level ('quasi-local')
- Recently filters/limiters have been introduced for shape-preserving tracer transport, however, reduces the transport operator from formally third-order to second-order.
- Under DOE grant we are integrating CSLAM into HOMME for tracer transport:
  - improve accuracy/efficiency of shape-preserving tracer transport

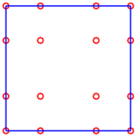

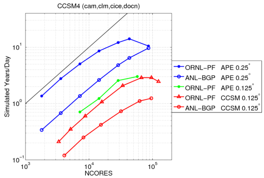

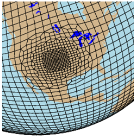

- Scalable spectral element dycore in CAM
  - fully functional with CAM4 physics; soon with mesh-refinement and CAM5 physics
- Conserves total energy to time truncation errors ($\approx$0.014 W/m^2 in $\frac{1}{2}^\circ$ aqua-planet)
- Conserves mass at the element level (‘quasi-local’)
- Recently filters/limiters have been introduced for shape-preserving tracer transport, however, reduces the transport operator from formally third-order to second-order.
- Under DOE grant we are integrating CSLAM into HOMME for tracer transport:
  - improve accuracy/efficiency of shape-preserving tracer transport
  - unique opportunity to compare computational efficiency/accuracy of finite-volume versus finite-element method within the same framework

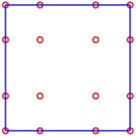

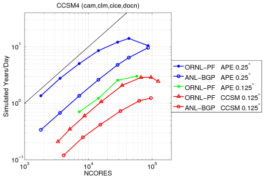

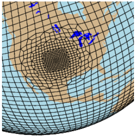

- Scalable spectral element dycore in CAM
  - fully functional with CAM4 physics; soon with mesh-refinement and CAM5 physics
- Conserves total energy to time truncation errors ($\approx$0.014 W/m^2 in $\frac{1}{2}^\circ$ aqua-planet)
- Conserves mass at the element level ('quasi-local')
- Recently filters/limiters have been introduced for shape-preserving tracer transport, however, reduces the transport operator from formally third-order to second-order.
- Under DOE grant we are integrating CSLAM into HOMME for tracer transport:
  - improve accuracy/efficiency of shape-preserving tracer transport
  - unique opportunity to compare computational efficiency/accuracy of finite-volume versus finite-element method within the same framework
    - CSLAM can take longer Δt's but needs a larger halo/stencil

CSLAM in CAM-HOMME (High-Order Methods Modeling Environment)

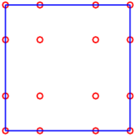

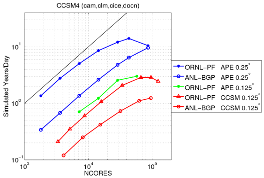

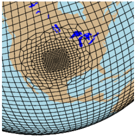

- Scalable spectral element dycore in CAM
  - fully functional with CAM4 physics; soon with mesh-refinement and CAM5 physics
- Conserves total energy to time truncation errors ($\approx$0.014 W/m^2 in $\frac{1}{2}^\circ$ aqua-planet)
- Conserves mass at the element level ('quasi-local')
- Recently filters/limiters have been introduced for shape-preserving tracer transport, however, reduces the transport operator from formally third-order to second-order.
- Under DOE grant we are integrating CSLAM into HOMME for tracer transport:
  - improve accuracy/efficiency of shape-preserving tracer transport
  - unique opportunity to compare computational efficiency/accuracy of finite-volume versus finite-element method within the same framework
    - CSLAM can take longer Δt's but needs a larger halo/stencil
    - HOMME must communicate between elements 3 times during one Δt but CSLAM only needs to communicate once

Commercial break

Springer book based on 2008 ASP summer colloquium on dynamical cores

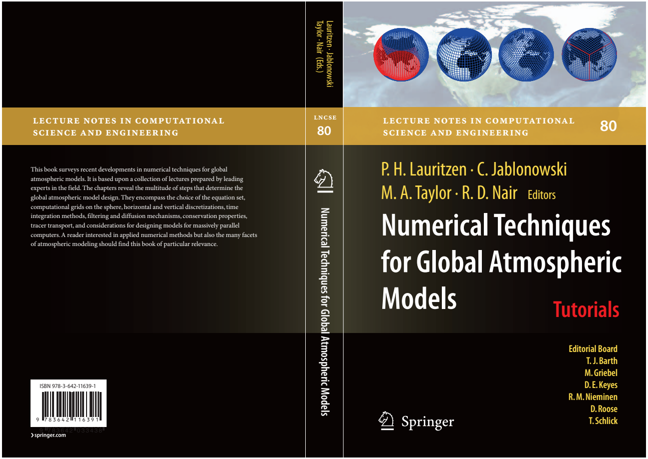

- 16 chapters (564 pp.) with contributions from J.Thuburn, D.Durran, J.Tribbia, B.Skamarock, T. Ringler, the editors, ...
- Expected publication date: early 2011

Part II
New challenging test cases for transport schemes on the sphere

Idealized transport test cases for global models in the literature

- Solid-body rotation (probably most widely used test case): purely translational

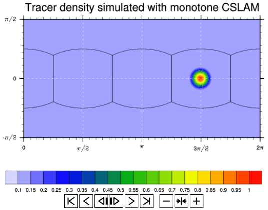

- Moving vortices (Nair and Jablonowski, 2008): translation+deformation

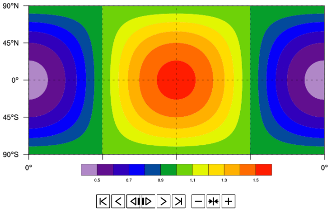

- Great-circle trajectories (analogous to straight lines on Cartesian plane)
  $\rightarrow$ this inherently favors most numerical schemes/methods
- No divergence/convergence
  $\rightarrow$ modelers basing their schemes on the flux-form of the continuity equations

$$\frac{\partial \rho}{\partial t} + \nabla \cdot (\vec{v}\rho) = 0, \tag{2}$$
$$\frac{\partial (\rho\,\phi)}{\partial t} + \nabla \cdot (\vec{v}\rho\,\phi) = 0, \tag{3}$$

  are not forced to distinguish between $\rho\,\phi$ and ϕ since

$$\frac{\partial \phi}{\partial t} + \nabla \cdot (\vec{v}\phi) = \phi \nabla \cdot \vec{v} = 0, \tag{4}$$

  for non-divergent flow $\nabla \cdot \vec{v} = 0$, that is, (3) and (4) take the same functional form.
- $\rightarrow$ Modelers are not forced to consider the coupling between tracer and air mass
- Single tracer tests and associated standard error norms do not address how well transport schemes preserve pre-existing functional relations between tracers.

More challenging class of idealized transport test cases for global models

To start addressing these issues we have developed a new class of test cases (Nair and Lauritzen, 2010)

However, for complex flows where parcel trajectories do not follow great-circle arcs (straight lines) closed-form analytic solutions are generally unavailable:

- so we follow ideas developed by LeVeque (1996): Time-reversing flow field, i.e. the exact solution at $t = T$ = initial condition ($t = 0$)

More challenging class of idealized transport test cases for global models

To start addressing these issues we have developed a new class of test cases (Nair and Lauritzen, 2010)

However, for complex flows where parcel trajectories do not follow great-circle arcs (straight lines) closed-form analytic solutions are generally unavailable:

- so we follow ideas developed by LeVeque (1996): Time-reversing flow field, i.e. the exact solution at $t = T =$ initial condition ($t = 0$)
- when flow reverses there is a potential for cancellation of errors! (will address this)

More challenging class of idealized transport test cases for global models

To start addressing these issues we have developed a new class of test cases (Nair and Lauritzen, 2010)

However, for complex flows where parcel trajectories do not follow great-circle arcs (straight lines) closed-form analytic solutions are generally unavailable:

- so we follow ideas developed by LeVeque (1996): Time-reversing flow field, i.e. the exact solution at $t = T =$ initial condition ($t = 0$)
- when flow reverses there is a potential for cancellation of errors! (will address this)
- parcels follow non-trivial trajectories $\Rightarrow$ high-order Taylor series expansions are used to compute 'exact' trajectories ('exact' for all practical purposes) $\Rightarrow$ flow can be used to assess accuracy of trajectory algorithms!

Flow field 1: non-divergent

The components of the velocity vector $\mathbf{V}(\lambda, \theta, t)$ is given by

$$u(\lambda, \theta, t) = \kappa \sin^2(\lambda') \sin(2\theta) \cos(\pi t/T) + 2\pi \cos(\theta)/T \quad (5)$$

$$v(\lambda, \theta, t) = \kappa \sin(2\lambda') \cos(\theta) \cos(\pi t/T), \quad (6)$$

respectively, where $T = 5$, $\kappa = 2$, and $\lambda' = \lambda - 2\pi t/T$

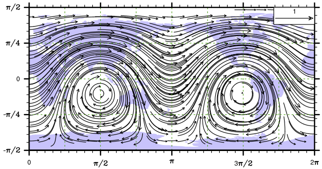

- for general applicability of the test case the wind field is defined in non-dimensional units (the problem can, of course, be dimensionalized for Earth).
- Wind field is formulated in terms of a deformational and translational component (and easy to implement):
  $\rightarrow$ translational component added so that potential cancellation of errors when flow reverses is eliminated

Flow field 1: non-divergent

The components of the velocity vector $\mathbf{V}(\lambda, \theta, t)$ is given by

$$u(\lambda, \theta, t) = \kappa \sin^2(\lambda') \sin(2\theta) \cos(\pi t/T) + 2\pi \cos(\theta)/T \quad (5)$$
$$v(\lambda, \theta, t) = \kappa \sin(2\lambda') \cos(\theta) \cos(\pi t/T), \quad (6)$$

respectively, where $T = 5$, $\kappa = 2$, and $\lambda' = \lambda - 2\pi t/T$

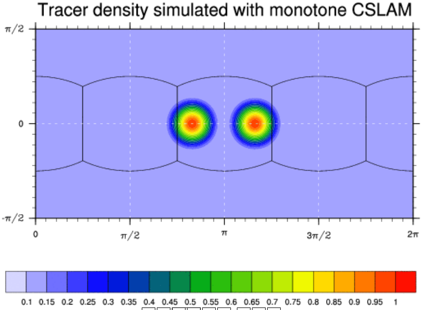

note that background value is non-zero; traditional test cases usually use zero

Flow field 1: non-divergent

The components of the velocity vector $\mathbf{V}(\lambda, \theta, t)$ is given by

$$u(\lambda, \theta, t) = \kappa \sin^2(\lambda') \sin(2\theta) \cos(\pi t/T) + 2\pi \cos(\theta)/T \qquad (5)$$

$$v(\lambda, \theta, t) = \kappa \sin(2\lambda') \cos(\theta) \cos(\pi t/T), \qquad (6)$$

respectively, where $T = 5$, $\kappa = 2$, and $\lambda' = \lambda - 2\pi t/T$

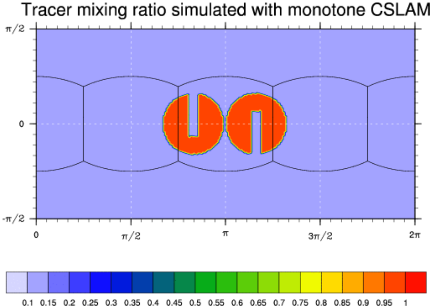

to challenge limiters under challenging flow conditions non-smooth initial condition can be used

Flow field 2: divergent

$\phi \in [0.1, 1]$ $\qquad$ $\rho\,\phi \in [0.1, 3.5]$ since $\rho(t) \neq 1$

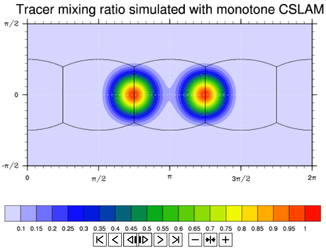

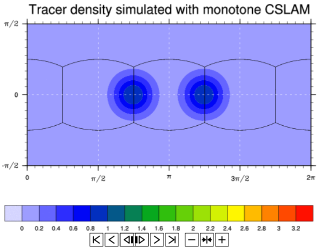

As far as I am aware this is the first global idealized transport test case using convergent-divergent winds!

Standard error norms

Since analytical solution is available (=initial conditions) at $t = T$ standard error norms can be computed:

$$\ell_2 = \left[\frac{I[(\phi - \phi_T)^2]}{I[(\phi_T)^2]}\right]^{1/2},$$
$$\ell_\infty = \frac{\max_{\forall\lambda,\theta}|\phi - \phi_T|}{\max_{\forall\lambda,\theta}|\phi_T|},$$

where ϕ_T, ϕ_0 are , respectively, the true solution and its initial value, and I is the global integral

These error norms 'only' measure global and maximum deviations from the truth!

How do these errors manifest themselves for interrelated species?

- important for stratospheric chemistry (next slide)
- important for cloud-aerosol interactions

  e.g., advection of a cloud boundary in which the spatial gradients of cloud condensation nuclei and cloud droplet mixing ratios are, in general, reversed (Ovtchinnikov and Easter, 2009)

Part III
New mixing diagnostic

Relationships between long-lived stratospheric tracers, manifested in similar spatial structures on scales ranging from a few to several thousand kilometers, are displayed most strikingly if the mixing ratio of one is plotted against another, when the data collapse onto remarkably compact curves. - Plumb (2007)

E.g., when plotting nitrous oxide (N_2O) against 'total odd nitrogen' (NO_y) or chlorofluorocarbon (CFC's)

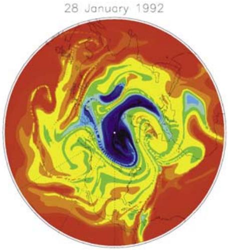

'inverse filling'

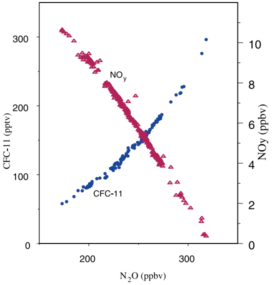

observations

Correlations between long-lived species in the stratosphere

Relationships between long-lived stratospheric tracers, manifested in similar spatial structures on scales ranging from a few to several thousand kilometers, are displayed most strikingly if the mixing ratio of one is plotted against another, when the data collapse onto remarkably compact curves. - Plumb (2007)

E.g., when plotting nitrous oxide (N_2O) *against 'total odd nitrogen'* (NO_y) *or chlorofluorocarbon* (CFC*'s*)

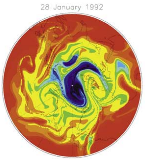

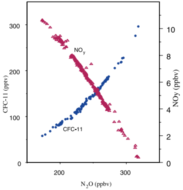

Transport operators may perturb pre-existing functional relationships
$\Rightarrow$ numerical mixing (may or may not be spurious)

Interrelated tracers

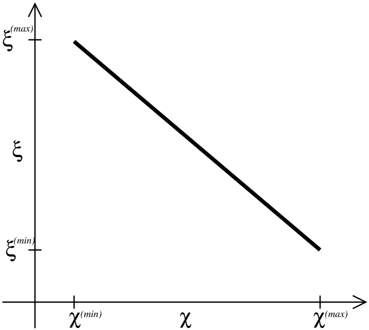

Analytical pre-existing functional relationship curve ψ (linear)

$$\xi = \psi(\chi) = a \cdot \chi + b, \quad \chi \in \left[\chi^{(min)}, \chi^{(max)}\right], \tag{7}$$

where a and b are constants, and χ and ξ are the mixing ratios of the two tracers

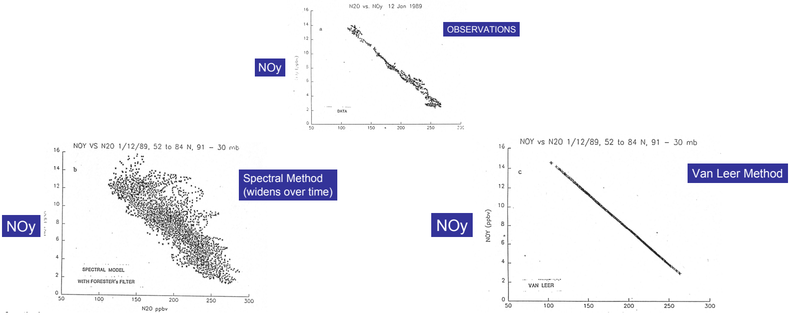

Figures from R.Rood's talk at the 2008 NCAR ASP colloquium

Analytical pre-existing functional relationship curve ψ (linear)

$$\xi = \psi(\chi) = a \cdot \chi + b, \quad \chi \in \left[\chi^{(min)}, \chi^{(max)}\right], \tag{7}$$

where a and b are constants, and χ and ξ are the mixing ratios of the two tracers

$\rightarrow$ carefully designed finite-volume schemes preserve linear correlations

(Lin and Rood, 1996; Thuburn and McIntyre, 1997)

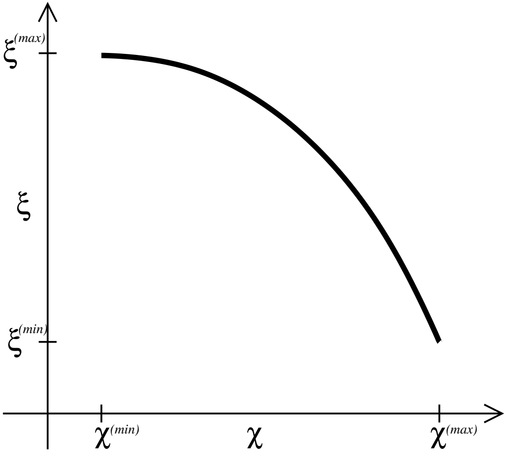

Analytical pre-existing functional relationship curve ψ

$$\xi = \psi(\chi) = a \cdot \chi^2 + b, \tag{8}$$

where a and b are constants so that ψ is concave or convex in $\left[\chi^{(min)}, \chi^{(max)}\right]$

Interrelated tracers

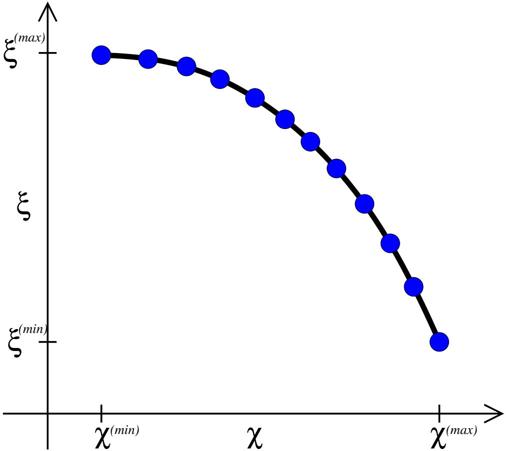

Discrete pre-existing functional relation (initial condition)

$$\xi_k = \psi(\chi_k) = a \cdot (\chi_k)^2 + b, \quad k = 1, .., K, \tag{8}$$

where a and b are constants so that ψ is concave or convex in $\left[\chi^{(min)}, \chi^{(max)}\right]$

Interrelated tracers

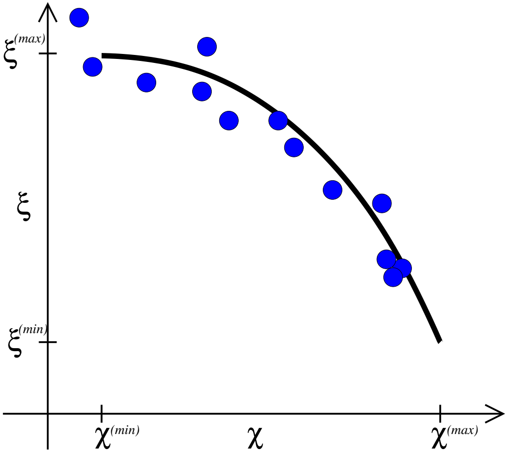

Any Eulerian/semi-Lagrangian scheme will disrupt pre-existing functional relation

$$\xi_k^{n+1} = \mathcal{T}(\xi_j^n) \neq a \cdot \mathcal{T}\left(\chi_j^n\right)^2 + b, \quad j \in \mathcal{H} \tag{8}$$

where $\mathcal{T}$ is the transport operator and $\mathcal{H}$ the set of indices defining the 'halo' for $\mathcal{T}$.

'Real' mixing, e.g., observed during polar vortex breakup (Waugh et al., 1997)

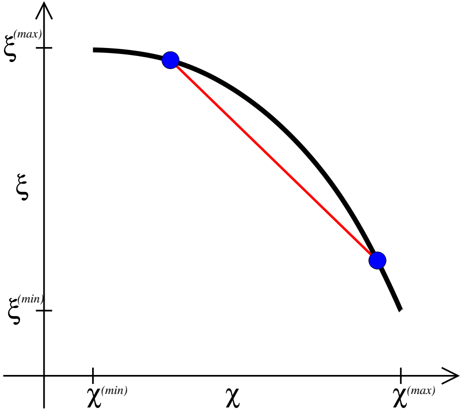

'Real mixing' (when occurring) will tend to replace the functional relation by a scatter by linearly interpolating along mixing lines between pairs of points
$\rightarrow$ ideally numerical mixing should = 'real mixing'!

'Real' mixing, e.g., observed during polar vortex breakup (Waugh et al., 1997)

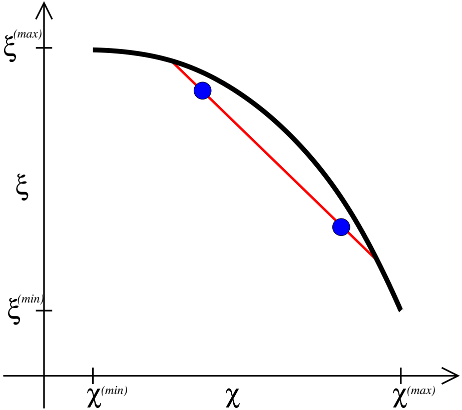

'Real mixing' (when occurring) will tend to replace the functional relation by a scatter by linearly interpolating along mixing lines between pairs of points
$\rightarrow$ ideally numerical mixing should = 'real mixing'!

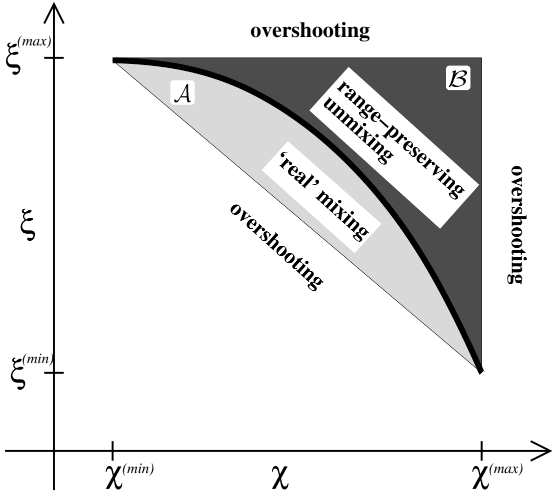
overshooting
$\xi^{(max)}$
$\mathcal{A}$
$\mathcal{B}$
range–preserving unmixing
'real' mixing
overshooting
overshooting
ξ
$\xi^{(min)}$
$\chi^{(min)}$
χ
$\chi^{(max)}$

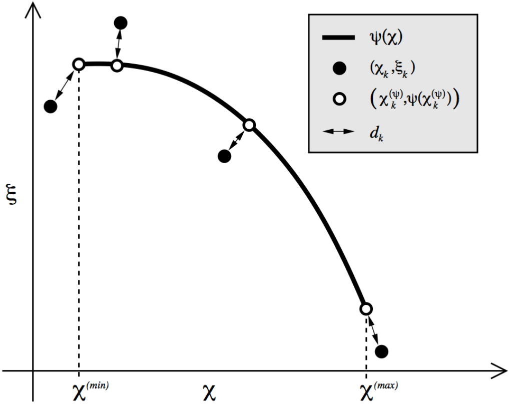

Figure 2. A schematic of d_k (left-right arrows) for different correlation points (χ_k, ξ_k) (filled circles) generated by the transport scheme. d_k is the 'normalized Euclidean distance' between (χ_k, ξ_k) and the point on the pre-existing functional relation $(\chi, \psi(\chi))$ (thick line), where $\xi \in [\chi^{(min)}, \chi^{(min)}]$ (dashed lines), nearest to (χ_k, ξ_k). This nearest point on $(\chi, \psi(\chi))$ is denoted $(\chi_k^{(\psi)}, \psi(\chi_k^{(\psi)})$ (unfilled circle).

Numerical mixing that resembles 'real' mixing in that values are shifted to the concave side of the pre-existing functional relation only

$$\ell_r = \frac{1}{K}\sum_{k=1}^{K}\begin{cases} d_k, & \text{if } (\chi_k, \xi_k) \in \mathcal{A} \\ 0, & \text{else} \end{cases} . \qquad (9)$$

Mixing that produces scatter points not in $\mathcal{A}$ is numerical unmixing.

Numerical mixing that resembles 'real' mixing in that values are shifted to the concave side of the pre-existing functional relation only

$$\ell_r = \frac{1}{K}\sum_{k=1}^{K}\begin{cases} d_k, & \text{if } (\chi_k, \xi_k) \in \mathcal{A} \\ 0, & \text{else} \end{cases}. \tag{9}$$

Mixing that produces scatter points not in $\mathcal{A}$ is numerical unmixing.

'Range-preserving' unmixing = numerical unmixing within the range of the initial data

$$\ell_u = \frac{1}{K}\sum_{k=1}^{K}\begin{cases} d_k, & \text{if } (\chi_k, \xi_k) \in \mathcal{B}, \\ 0, & \text{else.} \end{cases} \tag{10}$$

$\rightarrow$ shape-preservation constraint is not necessarily enough to guarantee $\ell_u = 0$.
$\rightarrow$ $\ell_u = 0 \Leftrightarrow$ semi-linear + monotone according to Harten (1983) (Thuburn and McIntyre, 1997);
$\rightarrow$ unfortunately, only first-order schemes will satisfy these constraints (Godunov, 1959).

Numerical mixing that resembles 'real' mixing in that values are shifted to the concave side of the pre-existing functional relation only

$$\ell_r = \frac{1}{K}\sum_{k=1}^{K}\begin{cases} d_k, & \text{if } (\chi_k, \xi_k) \in \mathcal{A} \\ 0, & \text{else} \end{cases}. \tag{9}$$

Mixing that produces scatter points not in $\mathcal{A}$ is numerical unmixing.

'Range-preserving' unmixing = numerical unmixing within the range of the initial data

$$\ell_u = \frac{1}{K}\sum_{k=1}^{K}\begin{cases} d_k, & \text{if } (\chi_k, \xi_k) \in \mathcal{B}, \\ 0, & \text{else.} \end{cases} \tag{10}$$

$\rightarrow$ shape-preservation constraint is not necessarily enough to guarantee $\ell_u = 0$.
$\rightarrow$ $\ell_u = 0 \Leftrightarrow$ semi-linear + monotone according to Harten (1983) (Thuburn and McIntyre, 1997);
semi-linear+monotone according to Harten (1983) is probably too strong a constraint!

Mixing diagnostics: 3 categories (Lauritzen and Thuburn, in prep.)

Numerical mixing that resembles 'real' mixing in that values are shifted to the concave side of the pre-existing functional relation only

$$\ell_r = \frac{1}{K}\sum_{k=1}^{K}\begin{cases} d_k, & \text{if } (\chi_k, \xi_k) \in \mathcal{A} \\ 0, & \text{else} \end{cases}. \tag{9}$$

Mixing that produces scatter points not in $\mathcal{A}$ is numerical unmixing.

'Range-preserving' unmixing = numerical unmixing within the range of the initial data

$$\ell_u = \frac{1}{K}\sum_{k=1}^{K}\begin{cases} d_k, & \text{if } (\chi_k, \xi_k) \in \mathcal{B}, \\ 0, & \text{else.} \end{cases} \tag{10}$$

$\rightarrow$ shape-preservation constraint is not necessarily enough to guarantee $\ell_u = 0$.
$\rightarrow$ $\ell_u = 0 \Leftrightarrow$ semi-linear + monotone according to Harten (1983) (Thuburn and McIntyre, 1997);
semi-linear+monotone according to Harten (1983) is probably too strong a constraint!

Overshooting (expanding range mixing)

$$\ell_o = \frac{1}{K}\sum_{k=1}^{K}\begin{cases} d_k, & \text{if } (\chi_k, \xi_k) \notin \mathcal{A} \text{ and } (\chi_k, \xi_k) \notin \mathcal{B}, \\ 0, & \text{else.} \end{cases}. \tag{11}$$

A scheme that is shape-preserving will result in $\ell_o = 0$.

Mixing diagnostics: 3 categories (Lauritzen and Thuburn, in prep.)

Numerical mixing that resembles 'real' mixing in that values are shifted to the concave side of the pre-existing functional relation only

$$\ell_r = \frac{1}{K}\sum_{k=1}^{K}\begin{cases} d_k, & \text{if } (\chi_k,\xi_k)\in\mathcal{A} \\ 0, & \text{else}\end{cases}. \tag{9}$$

Mixing that produces scatter points not in $\mathcal{A}$ is numerical unmixing.

'Range-preserving' unmixing = numerical unmixing within the range of the initial data

$$\ell_u = \frac{1}{K}\sum_{k=1}^{K}\begin{cases} d_k, & \text{if } (\chi_k,\xi_k)\in\mathcal{B}, \\ 0, & \text{else.}\end{cases} \tag{10}$$

$\rightarrow$ shape-preservation constraint is not necessarily enough to guarantee $\ell_u = 0$.
$\rightarrow$ $\ell_u = 0 \Leftrightarrow$ semi-linear + monotone according to Harten (1983) (Thuburn and McIntyre, 1997);
semi-linear+monotone according to Harten (1983) is probably too strong a constraint!

Overshooting (expanding range mixing)

$$\ell_o = \frac{1}{K}\sum_{k=1}^{K}\begin{cases} d_k, & \text{if } (\chi_k,\xi_k)\notin\mathcal{A} \text{ and } (\chi_k,\xi_k)\notin\mathcal{B}, \\ 0, & \text{else.}\end{cases}. \tag{11}$$

$\ell_o \neq 0$ can be 'poison' to parameterizations.

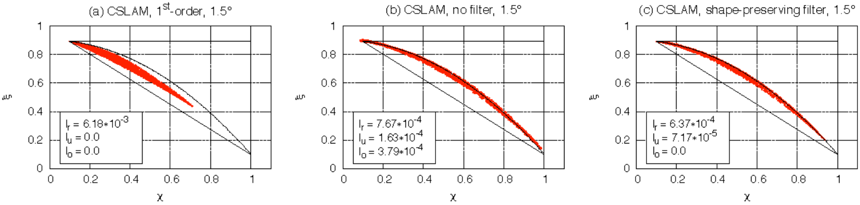

Setup

- Use deformational (and optionally divergent) flow that develops grid-scale features from well-resolved initial conditions.

Note: If simply using solid-body advection flow the transport operator is clearly not challenged enough:

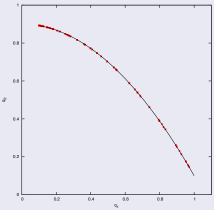

Mixing diagnostics: Results from CSLAM

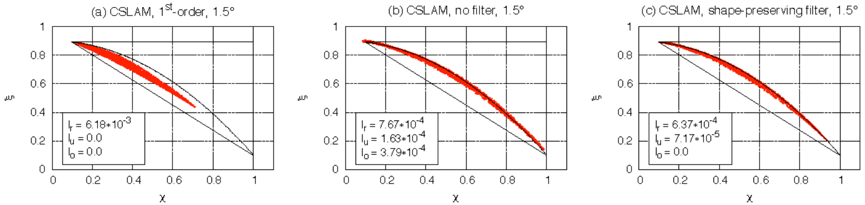

Setup

- Use deformational (and optionally divergent) flow that develops grid-scale features from well-resolved initial conditions.

  Note: If simply using solid-body advection flow the transport operator is clearly not challenged enough:

- here we used the nondivergent but strongly deformational flow
- cosine bells initial conditions
- compute mixing diagnostics half way through simulation (first part of simulation resembles atmospheric flow, however, not the latter part)
- note that mixing diagnostics do not require knowledge of the analytical solution

Mixing diagnostics: Results from CSLAM

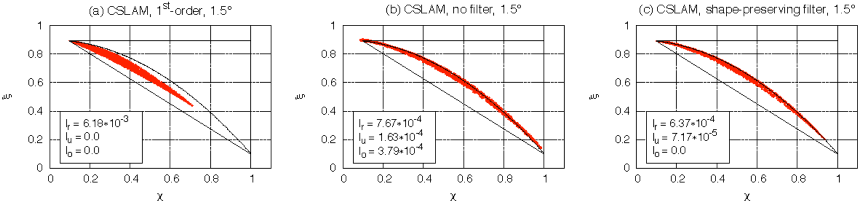

(a) 1^{st}-order version of CSLAM

- very diffusive: scatter points accumulate near scatter point for background values
- as predicted by theory: $\ell_u = 0$
- scheme is inherently shape-presersing: $\ell_o = 0$

(b) 3^{rd}-order version of CSLAM

- much less diffusive, however, $\ell_o \neq 0$ and $\ell_u \neq 0$

(b) 3^{rd}-order version of CSLAM with shape-preserving filter

- $\ell_o = 0$
- ℓ_r and ℓ_u are reduced further!

Mixing diagnostics: Results from CSLAM

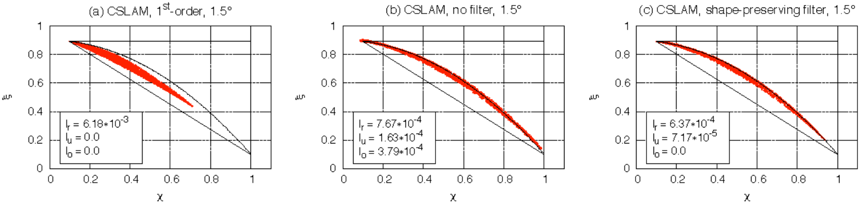

'Physically' motivated diagnostics

- NOTE: in terms of standard error norms (ℓ_2, ℓ_∞) shape-preserving CSLAM is less accurate than unlimited CSLAM whereas it is the other way around in terms of the mixing diagnostics.

- I believe the mixing diagnostics provide a 'physically' motivated metric to complement standard error measures to study numerical mixing, in particular, it provides an 'easy' framework to design better limiters/filters!


MLB.TV
COMMERCIAL BREAK
IN PROGRESS...

NCAR Workshop on Tracer Transport in March, 2011

The National Center for Atmospheric Research (NCAR) announces

Workshop on Transport Schemes on the Sphere

March 30 - 31, 2011, NCAR Mesa Lab, Boulder, Colorado, U.S.A.

Local Organizers are

Peter H. Lauritzen and William (Bill) Skamarock

Introduction

- The NCAR NESL divisions CGD and MMM as well as NCAR's IMAGe invite transport scheme developers to attend this "working" workshop on tracer transport schemes on the sphere. Participants are asked to give a presentation explaining the details of their transport scheme(s) and to present results from simulations using a newly developed test case suite for two-dimensional tracer transport on the sphere.

Overall goals

- Better understand the characteristics of different transport schemes
- Assess effective resolutions (for linear problems) with and without limiters/filters
- Discuss how to estimate accuracy versus computational cost (with and without limiters/filters)
- Investigate how well schemes maintain non-linear pre-existing functional relations

Test case setup

- Active participants are asked to bring solutions to one of the challenging test cases described in Nair and Lauritzen (2010)
- The test cases are easy to setup and formulated in terms of analytical winds and initial conditions:
  - 1 wind field: Non-divergent but highly deformational (Case 4 in Nair and Lauritzen, 2010)
  - 1 initial condition for air density: Unity everywhere
  - 4 initial conditions for tracer mixing ratio: Gaussian hills (smooth), cosine bells (quasi-smooth), slotted cylinders (non-smooth) and `correlated' cosine bells.
  - The wind field `reverses' half way through the simulation (t=T/2) so that the exact solution at the end of the simulation (t=T) is the initial condition. To avoid potential cancellation of errors by the flow reversal, a constant background flow is `added' to the time-reversing deformational flow.
  - Example animation of mixing ratio using slotted-cylinder initial conditions: movie
- A summary of simulations we ask modelers to perform is given in the table below:

Initial condition (IC)	Resolutions	Output	Purpose
Gaussian hills	Range from 3° to 0.2°	Standard error norms (t=T)	Assess numerical convergence rate for smooth IC without and with limiters/filters
Cosine hills	Range from 3° to 0.2°	Standard error norms (t=T)	Assess numerical convergence rate for quasi-smooth IC and define effective resolution N
Slotted cylinders	1.5°, 0.75°, N	Standard error norms (t=T) and contour plots (t=T/2,t=T)	Assess performance of scheme with `rough' IC without and with limiters/filters
Cosine hills and correlated cosine hills	1.5°, 0.75°, N	Mixing diagnostics and scatter plot at t=T/2	Assess ability of scheme to preserve nonlinear pre-existing functional relation without and with limiters/filters

- More details and specific guidance on the test case setup are given in this document: PDF (12.5 MB)

Code

- Fortran90 module for computing mixing diagnostics: diag.f90
- Gnuplot script to make convergence plot and perform least-squares linear regression to estimate numerical order of convergence: conv.gp, sample error-norm data file
- NCL script for contour plots which assumes the data is in ASCII format on a regular latitude-longitude grid: plot.ncl; sample data
- Gnuplot script to make scatter plot: corr.gp, sample data file and mixing bounds datafile

Practicalities

- Registration fee: None
- Abstract deadline: December 31, 2010 (please send a brief abstract describing your transport scheme to "tracer at cgd.ucar.edu").
- Notification of acceptance : January 15, 2011
- Hotel information: Coming soon

- How much 'real mixing' is appropriate for climate applications (ℓ_r threshold)? How much 'unmixing' can we tolerate (ℓ_o threshold)?
- Add 'toy' chemistry to new idealized test case: Two tracers that react with each other but should always add up to a constant
  Emulate, e.g., Br: Strong diurnal cycle (produced by photolysis)

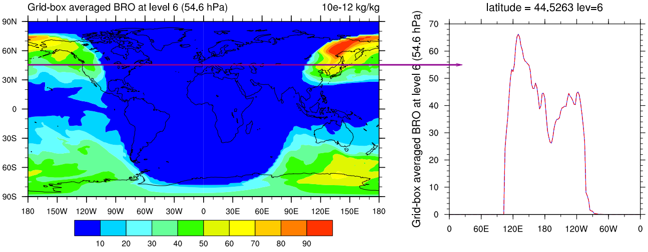

  → test development in progress - collaboration with NCAR-ACD (J.F.Lamarque, D. Kinnison)
- transport 3 or more tracers that add up to a constant with idealized wind fields (when advected individually the sum will not match the constant; e.g. total chlorine)

References I

Barth, T. and Jespersen, D. (1989). The design and application of upwind schemes on unstructured meshes. *Proc. AIAA 27th Aerospace Sciences Meeting, Reno.*

Blossey, P. N. and Durran, D. R. (2008). Selective monotonicity preservation in scalar advection. *J. Comput. Phys.*, 227(10):5160–5183.

Dukowicz, J. K. and Baumgardner, J. R. (2000). Incremental remapping as a transport/advection algorithm. *J. Comput. Phys.*, 160:318–335.

Godunov, S. K. (1959). A difference scheme for numerical computation of discontinuous solutions of equations in fluid dynamics. *Math. Sb.*, 47:271. Also: Cornell Aero. Lab. translation.

Harris, L. M., Lauritzen, P. H., and Mittal, R. (2010). A flux-form version of the conservative semi-Lagrangian multi-tracer transport scheme (CSLAM) on the cubed sphere grid. *J. Comput. Phys.* revising.

Harten, A. (1983). On the symmetric form of systems of conservation laws with entropy. *J. Comput. Phys.*, 49:151 – 164.

Lamarque, J. F., Kinnison, D. E., Hess, P. G., and Vitt, F. (2008). Simulated lower stratospheric trends between 1970 and 2005: Identifying the role of climate and composition changes. *J. Geophys. Res.*, 113(D12301).

Lauritzen, P., Jablonowski, C., Taylor, M., and Nair, R. D. (2010a). Rotated versions of the jablonowski steady-state and baroclinic wave test cases: A dynamical core intercomparison. *Journal of Advances in Modeling Earth Systems.* in press.

Lauritzen, P. H., Nair, R. D., and Ullrich, P. A. (2010b). A conservative semi-Lagrangian multi-tracer transport scheme (CSLAM) on the cubed-sphere grid. *J. Comput. Phys.*, 229:1401–1424.

Lauritzen, P. H. and Thuburn, J. (2010,in prep.). Evaluating advection/transport schemes using scatter plots and numerical mixing diagnostics.

LeVeque, R. J. (1996). High-resolution conservative algorithms for advection in incompressible flow. *SIAM J. Numer. Anal.*, 33:627–665.

Lin, S. J. and Rood, R. B. (1996). Multidimensional flux-form semi-Lagrangian transport schemes. *Mon. Wea. Rev.*, 124:2046–2070.

Nair, R. D. and Jablonowski, C. (2008). Moving vortices on the sphere: A test case for horizontal advection problems. *Mon. Wea. Rev.*, 136:699–711.

Nair, R. D. and Lauritzen, P. H. (2010). A class of deformational flow test cases for linear transport problems on the sphere. *J. Comput. Phys.*, 229:8868–8887.

Ovtchinnikov, M. and Easter, R. C. (2009). Nonlinear advection algorithms applied to interrelated tracers: Errors and implications for modeling aerosol-cloud interactions. *Mon. Wea. Rev.*, 137:632–644.

Plumb, R. A. (2007). Tracer interrelationships in the stratosphere. *Rev. Geophys.*, 45(RG4005).

Thuburn, J. and McIntyre, M. (1997). Numerical advection schemes, cross-isentropic random walks, and correlations between chemical species. *J. Geophys. Res.*, 102(D6):6775–6797.

Waugh, D. W., Plumb, R. A., Elkins, J. W., Fahey, D. W., Boering, K. A., Dutton, G. S., Volk, C. M., Keim, E., Gao, R.-S., Daube, B. C., Wofsy, S. C., Loewenstein, M., Podolske, J. R., Chan, K. R., Proffitt, M. H., Kelly, K. K., Newman, P. A., and Lait, L. R. (1997). Mixing of polar vortex air into middle latitudes as revealed by tracer-tracer scatterplots. *J. Geophys. Res.*, 120(D11):119–134.

Zalesak, S. T. (1979). Fully multidimensional flux-corrected transport algorithms for fluids. *J. Comput. Phys.*, 31:335–362.